Medicon Engineering Themes
Volume 3 Issue 3 September 2022
Research Article

Numerical Study on Thermohydraulic Characteristics of Reciprocating Room Temperature Active Magnetic Regenerator

Georges El Achkar[1,2]*, B Liu[1] and R Bennacer[1,3]

[1]*Tianjin University of Commerce, Guangrong Rd 409, Beichen District, Tianjin, 300134, China*

[2]*Calyos, 20 Zoning De Jumet, 6040 Charleroi, Belgium*

[3]*ENS Paris-Saclay University, 61 Avenue du Président Wilson, 94235 Cachan, France*

***Corresponding Author:** Georges El Achkar, Tianjin University of Commerce, Guangrong Rd 409, Beichen District, Tianjin, 300134, China; Calyos, 20 Zoning De Jumet, 6040 Charleroi, Belgium.

Received: August 11, 2022; **Published:** August 30, 2022

DOI: 10.55162/MCET.03.076

Abstract

In this paper, a thermohydraulic characterisation of a reciprocating room temperature active magnetic regenerator, with gadolinium particles used as a magnetocaloric material and water used as a heat transfer fluid, was numerically carried out. A two-dimensional transient flow model was developed using COMSOL Multiphysics software in order to determine the water flow distribution in two active magnetic regenerators of cross and parallel gadolinium particles distributions for different water inlet velocities of 0.06, 0.08, 0.1 and 0.12 $m.s^{-1}$. The gadolinium particles have a radius of 1.5 mm and a distance from one another of 0.9 mm. Based on the simulations results of this model, a second two-dimensional transient coupled flow and heat transfer model was then developed using the same software in order to characterise the convective heat transfer in the active magnetic regenerator of cross gadolinium particles distribution for the same water inlet velocities.

Keywords: Magnetic refrigeration; active magnetic regenerator; magnetocaloric material; gadolinium; magnetocaloric effect; flow distribution; heat transfer; modelling

Nomenclatures

AMR: active magnetic regenerator.
C_p: specific heat capacity, $J.kg^{-1}.K^{-1}$.
D_h: hydraulic diameter of the AMR, m.
g: gravity acceleration, $m.s^{-2}$.
Gd: gadolinium.
H: distance between particles, m.
HS: heat source, J.
L: length of the AMR, m.
m: mass flow rate at AMR inlet, $kg.s^{-1}$.
MCE: magnetocaloric effect.
MCM: magnetocaloric material.
Nu: Nusselt number.
P: relative pressure, Pa.

P_r: Prandtl number.
q: heat flux, W.m^{-2}.
r: radius of particles, m.
Re: Reynolds number.
S: cross-sectional area of AMR, m^2.
T: time, s.
T: temperature, °C.
u: velocity in x-axis direction, m.s^{-1}.
U: velocity at the AMR inlet, m.s^{-1}.
v: velocity in y-axis direction, m.s^{-1}.

Greek symbols

Γ: thermal diffusion coefficient, m^2.s^{-1}.
Λ: thermal conductivity, W.m^{-1}.K^{-1}.
μ: dynamic viscosity, Pa.s.
ϕ: general variable.
ρ: density, kg.m^{-3}.

Subscripts

Out: outlet.
W: water.
F: fluid.
0: initial.

Introduction

The growing need for cooling, refrigeration and air conditioning requires an increasing use of two- phase thermal systems, such as heat pumps, capillary pumped loops or loop heat pipes. Nevertheless, these systems have the disadvantage of operating with refrigerants, which often have a negative impact on the ozone layer and/or a significant contribution to the greenhouse effect [1, 2, 3]. The quality of new environmentally friendly refrigerants will probably be to the detriment of the thermal performance and/or the stability of these systems [3, 4, 5]. It is therefore important to search for new cold production solutions ensuring low environmental impact and high thermal efficiency and stability.

In this context, the magnetic refrigeration technology, based on the magnetocaloric effect (MCE), appears as a potentially viable solution [6, 7, 8, 9, 10]. This relatively new technology has several advantages but few drawbacks with respect to two-phase thermal systems [10, 11]. As for the advantages, the theoretical optimal coefficient of performance (COP) of this technology is of the same order as that of two-phase thermal systems. In addition, this technology operates with water at low pressure and frequency, which is convenient for the environment, the security, the maintenance cost, the noise and the lifetime. However, this technology involves rare earth magnetocaloric materials (MCMs), which are less available and very expensive, and its initial cost is higher than that of two- phase thermal systems.

The MCE, discovered by Weiss and Picard [12, 13, 14, 16] in 1917, is a physical phenomenon occurring in a MCM under the influence of a varying magnetic field (H) [15]. It is usually expressed as an adiabatic temperature change (ΔT_{ad}) or an isothermal total entropy change (ΔS_{tot}) of the MCM. In the absence of a magnetic field (H=0 T), the magnetic moments in the MCM are disordered (Fig. 1a). If a magnetic field is applied (H>0 T), the magnetic moments in the MCM are forced to align in a higher order (Fig. 1b). As a consequence, the magnetic entropy (S_m) decreases. In isentropic (i.e. adiabatic) conditions, the total entropy ($S_{tot} = S_m + S_l$) remains constant. There-

fore, the decrease of the S_m manifests itself in an increase of the lattice entropy (S_l). The atoms in the material vibrate more intensively and hence, the temperature of the MCM increases. The opposite occurs when the magnetic field is removed. The S_m increases and so the S_l decreases, leading to a decrease of the MCM temperature. It is worth noting that the ΔS_m and the ΔT_{ad} attain their maximum values at the temperature corresponding to the magnetic phase change called the Curie temperature (T_c).

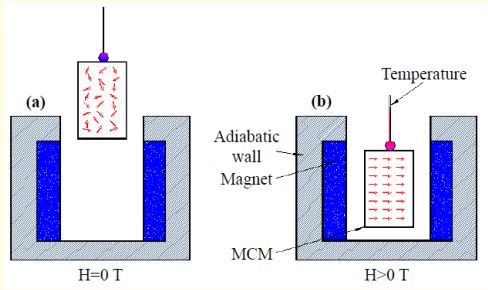

Figure 1: Schematic diagram of the MCE principle; (a) H=0 T; (b) H>0 T.

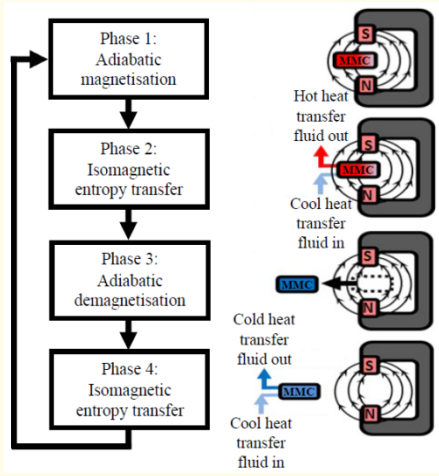

Figure 2: Schematic diagram of the AMR operation cycle.

It is well known that the MCE of most MCMs at moderate magnetic fields (up to 1.5 T) is limited to a maximum ΔT_{ad} of 5°C [17, 18]. This value is not sufficient for such materials to be directly implemented into a practical refrigeration system where a much greater temperature span could be required. Therefore, in order to increase the temperature span, the best solution is to integrate an active magnetic regenerator (AMR) in the magnetic refrigeration system. The operation cycle of this AMR is generally based on four thermodynamic processes (Fig. 2):

- Adiabatic magnetisation (phase 1): At the initial cycle time, the MCM at room temperature is put under a magnetic field, causing a uniform increase of its temperature relative to its ΔT_{ad} under the effect of the atomic magnetic moments alignment.
- Isomagnetic transfer of entropy (phase 2): At the second cycle time, a cool heat transfer fluid circulation is imposed through the MCM (always in presence of a magnetic field), so the heat transfer fluid recovers the heat from the MCM and hence the heat transfer fluid heats up and the MCM cools down.

- Adiabatic demagnetisation (phase 3): At the third cycle time, the heat transfer fluid circulation is stopped and the magnetic field is removed, causing a uniform decrease of the MCM temperature.
- Isomagnetic transfer of entropy (phase 4): At the final cycle time, a cool heat transfer fluid circulation is imposed through the MCM (always in absence of a magnetic field), so the heat transfer fluid releases the heat to the MCM and hence the heat transfer fluid cools down and the MCM heats up.

In this work, a numerical thermohydraulic characterisation of a reciprocating room temperature AMR was performed by developing two flow and heat transfer models, allowing the determination of the heat transfer fluid (water) flow distribution and the heat transfer with the MCM (Gd) for different operating conditions.

Modelling

Flow model

A two-dimensional transient flow model was developed using COMSOL Multiphysics software [20] in order to determine the water flow distribution in two AMRs of cross and parallel Gd particles distributions for different water inlet velocities.

A physical model of the magnetocaloric system was first established. A grid with a high refinement was then created. It should be noted that the obtained results showed a complete quantitative independence of the grid refinement, however, a higher grid refinement resulted in better qualitative results. Afterwards, the boundary conditions were imposed according to the operating conditions of the magnetocaloric system, taking into account some simplifying assumptions. The simulations were finally run with different boundary conditions and the results were extracted.

Physical model

The physical model of the magnetocaloric system mainly consisted of an AMR and a movable permanent magnet (Fig. 3).

The AMR was splitted into two symmetrical cylinders (Fig. 4) in order to enhance its heat transfer efficiency. These cylinders were designed according to the AMR configuration considered by Kawanami et al. [19] (Fig. 5). The permanent magnet alternatively moves towards the left and right cylinders, inducing thus their alternative magnetisation and demagnetisation. When the permanent magnet covers one cylinder, the magnetised Gd of this cylinder heats up, while the demagnetised Gd of the other cylinder cools down. Likewise, the water alternatively flows in the two directions through the AMR during the operation cycle phases 2 and 4 to exchange heat with the Gd.

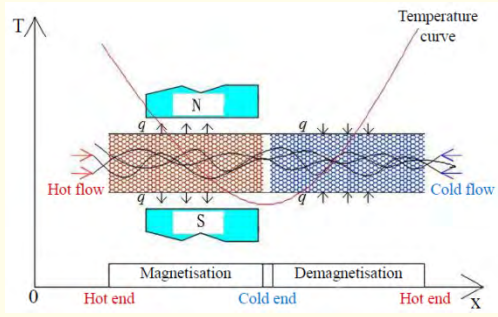

Figure 3: Physical model of the magnetocaloric system.

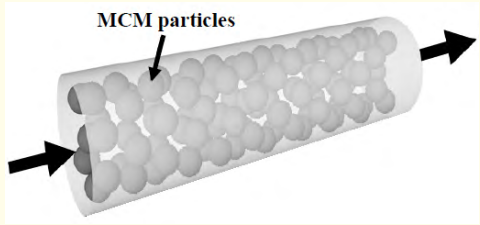

Figure 4: Schematic diagram of the AMR cylinder.

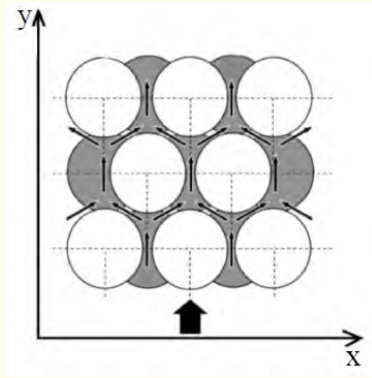

Figure 5: Configuration of the AMR considered by Kawanami et al. [19]

Assumptions

In order to simplify the mathematical formulation and the resolution of the flow model, several assumptions were considered:

- The water is incompressible;
- The water flow is laminar;
- No slip condition at the particle surface;
- The thermophysical properties of the Gd and the water remain constant regardless of their temperature and the magnetic field;
- The singular pressure drop of the water at the AMR inlet is neglected.

Mathematical model

Based on the previous assumptions, the continuity and momentum equations are written as follows:

Continuity equation:

$$\frac{\partial u_w}{\partial x} + \frac{\partial v_w}{\partial y} = 0 \qquad (1)$$

Momentum equations in x-axis and y-axis directions:

$$\rho_w \left(u_w \frac{\partial u_w}{\partial x} + v_w \frac{\partial u_w}{\partial y} \right) = -\frac{\partial p_w}{\partial x} + \mu_w \left(\frac{\partial^2 u_w}{\partial x^2} + v_w \frac{\partial^2 u_w}{\partial y^2} \right) \quad (2)$$

$$\rho_w \left(u_w \frac{\partial v_w}{\partial x} + v_w \frac{\partial v_w}{\partial y} \right) = -\frac{\partial p_w}{\partial x} + \mu_w \left(\frac{\partial^2 v_w}{\partial x^2} + v_w \frac{\partial^2 v_w}{\partial y^2} \right) - \rho_w g \quad (3)$$

Where u_w and v_w are the velocities of the water in the x&y-axis directions, respectively, and ρ_w, p_w and μ_w are the density, the relative pressure and the dynamic viscosity of the water, respectively.

For the calculation of the AMR hydraulic diameter (D_h), the following correlation corresponding to a similar particles structure proposed by Vuarnoz and Kawanami [21] was used:

$$D_h = \frac{2\left(2\sqrt{3} - \pi\right)}{\pi} r_{Gd} \quad (4)$$

Where r_{Gd} is the Gd particles radius.

Knowing the D_h, the water velocity at the AMR inlet (U_w) can be calculated as follows:

$$U_w = \frac{\dot{m}_w}{\rho_w S} = \frac{4\dot{m}_w}{\pi \rho_w D_h^2} \quad (5)$$

Where m_w is the mass flow rate of the water at the AMR inlet and S is the cross-sectional area of the AMR.

Numerical simulations

In the numerical simulations, two parallel and cross Gd particles distributions in the AMR were adopted and the conditions reported in Table 1 were considered. The water mass flow rate was chosen so that the Reynolds number (Re_w) was lower than 2000 in order to ensure a laminar flow.

Parameter (unit)	***Value***
S (m^2)	0.0008
T_0 (K)	291.15
μ_w (Pa.s)	1.006×10^{-3}
λGd (W.m−1.K−1)	10.6
cp,Gd (J.kg−1.K−1)	235.5
r_{Gd} (mm)	1.5
H_{Gd} (mm)	0.9
$p_{w,out}$ (Pa)	0
U_w ($m.s^{-1}$)	0.06; 0.08; 0.1; 0.12

Table 1: Numerical simulations conditions.

Results and Discussion

Fig. 6 shows the water flow distribution in the AMRs of cross and parallel Gd particles distributions for different water inlet velocities.

In the case of cross Gd particles distribution (Fig. 6a), for water inlet velocities of 0.06 and 0.08 $m.s^{-1}$, no Eddy flow was generated in the AMR. For water inlet velocity higher than 0.1 $m.s^{-1}$, the Eddy flow obviously appeared in the right half of the AMR. This phenomenon caused the water to stagnate in the convective heat transfer zones, which is not conducive to the heat transfer process. Indeed, when the water flows around the spherical surface of the particle, the flow is accelerated in the left half of the curved particle surface and the streamlines outside the boundary layer can be considered as a potential flow. The flow velocity between the particles is relatively high and the pressure is low. The water pressure in the boundary layer is consistent with the flow direction and its gradient overcomes the viscous force between the water and the curved surface. The water in this interval is not separated from the boundary layer, and hence, it can fully exchange heat with the particle. When the fluid flows through the right half of the curved particle surface, the water velocity decreases and the pressure increases in the flow direction. Under the action of the back pressure gradient, the water reflows and pushes its particles away from the curved surface, which leads to a formation of a boundary layer separation. Therefore, for the considered AMR configuration, the optimal water inlet velocity was $m.s^{-1}$ for a convenient convective heat transfer between the water and the Gd particles. In the case of parallel Gd particles distribution (Fig. 6b), the main water flow passes in the x-axis direction through the space between the particles and a small water flow passes in the y-axis direction through the gap between the particles. Therefore, the heat exchange between the water and the Gd particles mainly occurs through the upper and lower surfaces of the particles. Compared with the cross Gd particles distribution structure, this structure cannot effectively transfer the heat from the particles to the water, reducing thus the heat transfer performance of the AMR.

Fig. 7 shows the evolutions of the water pressure gradient in the x-axis direction as a function of the water inlet velocity in the AMRs of cross and parallel MCM particles distributions.

The overall trends of the pressure gradient curves in the two cases are similar, however, the pressure gradient in the cross Gd particles distribution case is significantly higher than that of the parallel Gd particles distribution case. This can be explained by the greater complexity of the cross Gd particles distribution configuration, inducing higher singular and frictional pressure drop.

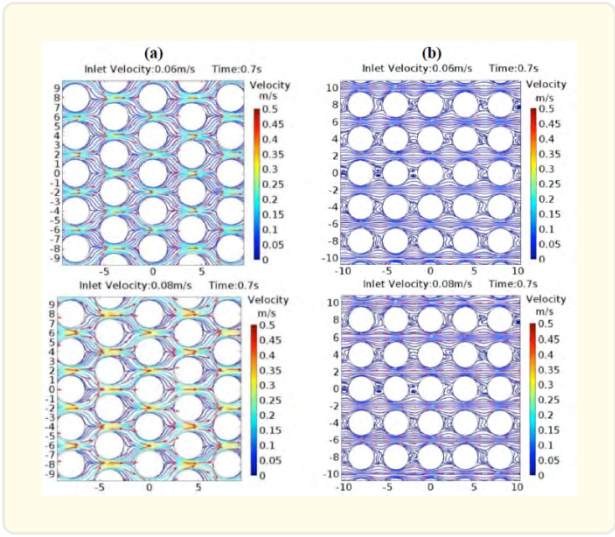

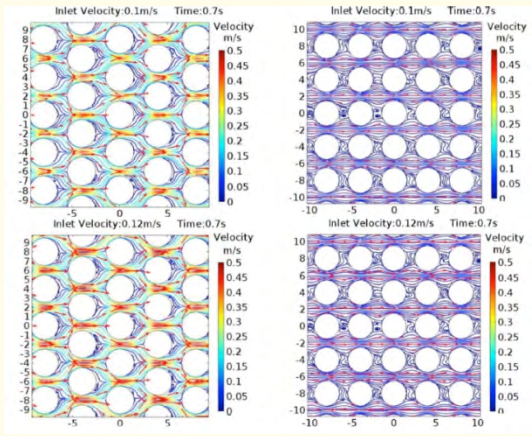

Figure 6: Water flow distribution in the AMRs of (a) cross and (b) parallel Gd particles distributions for different water inlet velocities.

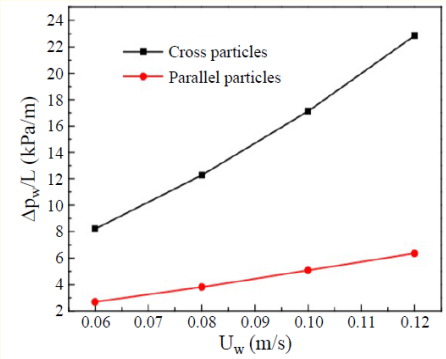

Figure 7: Evolutions of the water pressure gradient in the x-axis direction as a function of the water inlet velocity in the AMRs of cross and parallel MCM particles distributions.

Flow and heat transfer model

Based on the numerical simulations results of the presented flow model, a two-dimensional transient coupled flow and heat transfer model was developed using COMSOL Multiphysics software in order to characterise the convective heat transfer process in the AMR of cross Gd particles distribution for different water inlet velocities. The same modelling procedure of the magnetocaloric system as that presented in the flow model was adopted.

Physical model

The physical model considered in this model is similar to that of the flow model.

Assumptions

In order to simplify the mathematical formulation and the resolution of the flow and heat transfer model, several assumptions were considered:

- The water is incompressible;
- No slip condition at the particle surface;
- The thermophysical properties of the Gd and the water remain constant regardless of their temperature and the magnetic field;
- The thermal processes in the AMR occur under adiabatic boundary conditions;
- The heat losses are neglected.

Mathematical model

Based on the previous assumptions, the governing equation is written as follows:

$$\frac{\partial(\rho_w \phi)}{\partial t} + \frac{\partial(\rho_w u_w \phi)}{\partial t} + \frac{\partial(\rho_w v_w \phi)}{\partial t} = \frac{\partial}{\partial x}\left(\Gamma_w \frac{\partial \phi}{\partial x}\right) + \frac{\partial}{\partial y}\left(\Gamma_w \frac{\partial \phi}{\partial y}\right) + HS \qquad (6)$$

On the basis of the flow model, the heat source (*HS*) representing the sensible heat inside the Gd particles (i.e. proportional to ΔT_{ad}) was added.

Numerical simulations

In order to carry out the numerical simulations, the value of the ΔT_{ad} of the Gd was determined thanks to a specific experimental measurement method. A ΔT_{ad} of 3.5°C was found for Gd at a room temperature of 18°C under a magnetic field of 1.5 T. The inlet water temperature was set at 18°C and the Prandtl number was set at 7.5. Different water inlet velocities of 0.06, 0.08, 0.1 and 0.12 m.s^{-1} were chosen to simulate the convective heat transfer process in the AMR.

Results and discussion

Fig. 8 shows the temperature distribution in the AMR for water inlet velocity of 0.1 m.s^{-1} and initial temperature of 18°C. It was found that the temperature distribution at the AMR inlet was uniform. When the water flowed around the particles along the AMR, its temperature close to the particles raised and the temperature of the particles back surface was relatively high because of the water back-flow. The breakup of the thermal boundary layer caused by the Eddy phenomenon enhanced the heat transfer between the Gd and the water. However, the energy was trapped due to the relatively short convective heat transfer time (Fig. 9) and the convective heat transfer was weakened. In addition, the increase of the water inlet velocity leaded to an increase of the convective heat transfer.

Fig. 10 shows the evolutions of water velocity as a function of the position in the x-axis direction around the Gd particle for different inlet velocities. The water velocity trend was qualitativement the same for all the inlet velocities. The flow first accelerated in the particle left half and then decelerated in the right particle half, as found previously. Owing to the boundary layer separation caused by the presence of the Eddy flow, the water velocity in the x-axis direction approached to zero.

In order to further analyse the convective heat transfer process around the particles, the Nusselt number (N_u) in the x-axis direction was analysed and calculated at the same position of the water velocity shown previously. First, the Prandtl number (P_r) was calculated by the one-dimensional plot group in the COMSOL Multiphysics software. The N_u was calculated by the water flow velocity curve and the P_r curve near the surface of the particle as follows:

$$Nu = 0.35\left(\frac{S_1}{S_2}\right)^{0.2} Re_w^{0.6} Pr_w^{0.36}\left(\frac{Pr_w}{Pr_w}\right)^{0.25} \qquad (7)$$

Where S_1 = 4 mm and S_2 = 3.5 mm.

Fig. 11 shows the evolutions of the N_u as a function of the position in the x-axis direction around the Gd particle for different water inlet velocities. It can be seen that the N_u first increased in the particle left half and then decreased in the right particle half regardless of the water inlet velocity, which is coherent with the trend of the water velocity. In addition, an increase of the water inlet velocity increased the local velocity and hence the local N_u. The best way to enhance the convective heat transfer between the particles and the water is thus, other than increasing the heat exchange surface, to increase the inlet velocity and the mixing of the water.

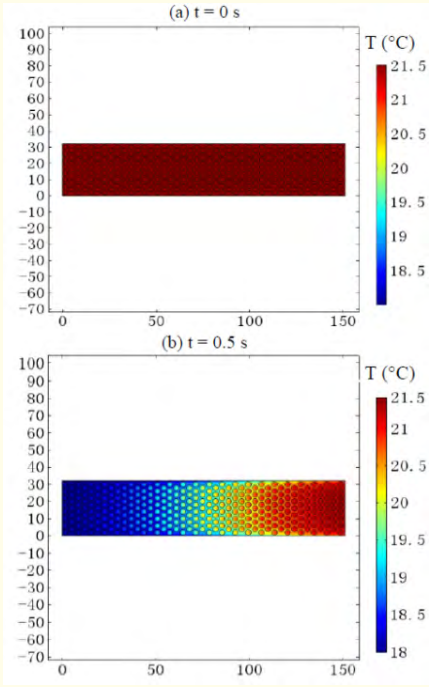

Figure 8: Temperature distribution in the AMR of cross Gd particles distribution for water inlet velocity of 0.1 m.s^{-1} and initial temperature of 18°C at (a) t = 0 s and (b) t = 0.5 s.

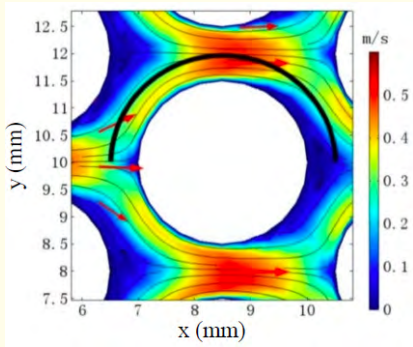

Figure 9: Water velocity distribution around a Gd particle.

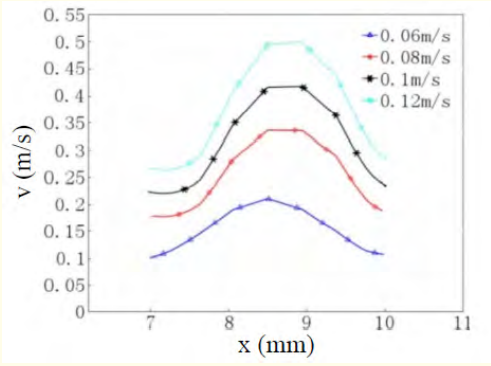

Figure 10: Evolutions of water velocity as a function of the position in the x-axis direction around a Gd particle for different water inlet velocities.

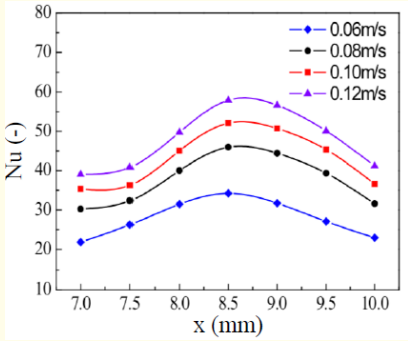

Figure 11: Evolutions of N_u as a function of the position in the x-axis direction around a Gd particle for different water inlet velocities.

Conclusions and Perspectives

A numerical study on the thermohydraulic performance of a reciprocating room temperature AMR was conducted. Two-dimensional transient flow and coupled flow and heat transfer models were developed using COMSOL Multiphysics, in order to characterise the flow and the convective heat transfer in two AMRs of parallel and cross Gd particles distributions. The water flow distribution and pressure drop in the AMR were determined in the two configurations showing that the cross Gd particles distribution was more advantageous for the water mixing and the breakup of the thermal boundary layer, which leads to an enhancement of the convective heat transfer.

As perpectives to this work, different AMR geometries and MCMs will be studied in order to optimise the convective heat transfer while ensuring a lowest pressure drop possible.

Acknowledgments

Financial support from the National Natural Science Foundation of China (No. 51706154) is gratefully acknowledged.

References

1. Wuebbles DJ. "The role of refrigerants in climate change". International Journal of Refrigeration 17.1 (1994): 7-17.
2. Khetib Y, Meniai A-H and Lallemand A. "Computer-aided design of CFC and HCFC substitutes using group contribution methods". Desalination 239 (2009): 82-91.
3. Benhadid-Dib S and Benzaoui A. "Refrigerants and their environmental impact Substitution of hydro chlorofluorocarbon HCFC and HFC hydro fluorocarbon". Search for an adequate refrigerant. Energy Procedia 18 (2012): 807-816.
4. Bivens DB and Minor BH. "Fluoroethers and other next generation fluids". International Journal of Refrigeration 21.7 (1998): 567-576.
5. Current long-term alternative refrigerants and their possible applications. 31st Informatory Note on Refrigeration Technologies. International Institute of Refrigeration (2016).
6. Russek SL and Zimm CB. "Potential for cost effective magnetocaloric air conditioning systems". International Journal of Refrigeration 29.8 (2006): 1366-1373.
7. Sari O and Balli M. "From conventional to magnetic refrigerator technology". International Journal of Refrigeration 37 (2014): 8-15.
8. Mezaal NA, Osintsev KV and Zhirgalova TB. "Review of magnetic refrigeration system as alternative to conventional refrigeration system". IOP Conference Series: Earth and Environmental Science 87 (2017): 032024.
9. Franco V., et al., "Magnetocaloric effect: From materials research to refrigeration devices". Progress in Materials Science 93 (2018): 112- 232.
10. Ansolia A and Arya M. "Magnetic refrigeration: A promising substitute for vapour compression system". International Journal of Innovations in Engineering and Technology 8.2 (2017): 180-186.
11. Singal LC, Mahajan A and Singh R. "Magnetic Refrigeration- A Review- A boon for the coming generations". SSRG International Journal of Mechanical Engineering 3.5 (2016): 23-29.
12. Warburg EG. "Magnetic investigations of physics (Leipzig). About some effects of the coercive force. annals13 (1881): 141-164.
13. Weiss P and Piccard A. "The magnetocaloric phenomenon". Journal of Theoretical and Applied Physics 7.1 (1917): 103-109.
14. Weiss P and Piccard A. On a new ph. magnetocaloric phenomenon. Reports 166 (1918): 352-354.
15. Kitanovski A., et al. "Magnetocaloric Energy Conversion: From Theory to Applications". Green energy and technology (2015).
16. Smith A. "Who discovered the magnetocaloric effect?". The European Physical Journal H 38.4 (2013): 507-517.
17. Gschneidner Jr KA, Pecharsky VK and Tsokol AO. "Recent development in magnetocaloric materials". Reports on Progress in Physics 68.6 (2005): 1479-1539.
18. Bruck E., et al. "Magnetocaloric refrigeration near room temperature (invited)". Journal of Magnetism and Magnetic Materials 310.2 (2007): 2793-2799.
19. Kawanami T., et al. "Optimization of a magnetic refrigerator at room temperature for air cooling systems". International Journal of Refrigeration 29.8 (2006): 1294-1301.
20. Whitaker S. "Flow in porous media I: A theoretical derivation of Darcy's law". Transport in Porous Media 1.1 (1986): 3-25.
21. Vuarnoz D and Kawanami T. "Numerical analysis of a reciprocating active magnetic regenerator made of gadolinium wires". Applied Thermal Engineering 37.2 (2012): 388-395.

Volume 3 Issue 3 September 2022